

ATOMIC DATA AND SPECTRAL LINE INTENSITIES FOR Mg VIII

A. K. BHATIA AND ROGER J. THOMAS

Laboratory for Astronomy and Solar Physics, Code 682, NASA/Goddard Space Flight Center, Greenbelt, MD 20771

Received 1997 April 28; accepted 1997 November 11

ABSTRACT

EUV spectral lines of Mg VIII have been observed from the solar corona by *Skylab*, *SERTS*, and more recently by *SOHO*. Atomic data for this astrophysically important ion are presented in this paper. The atomic data include energy levels, oscillator strengths, transition rates, and electron-impact excitation collision strengths. Twenty levels are included by using the configurations $2s^22p$, $2s2p^2$, $2p^3$, $2s^23s$, $2s^23p$, and $2s^23d$. Collision strengths are calculated at five incident energies (15.0, 22.5, 30.0, 37.5, and 45.0 Ry) in the distorted wave approximation. The temperature of maximum abundance for this ion is $\log T_e = 5.9$ K. The rate coefficients are calculated at this temperature by averaging the collision strengths over a Maxwellian distribution. Proton rates and solar background radiation have been included in calculating level populations, and intensity ratios are calculated by including proton rates only. The relative intensity ratios are compared with observed ratios obtained from *SERTS* and *SOHO/CDS* to infer electron density in different solar features such as an active region, quiet-Sun, and off-limb. With a few exceptions, the predicted intensity ratios match observed values very well over a variety of instrumentation and solar conditions. Since Mg VIII has a number of strong EUV lines, we expect that the spectra of this ion should prove useful for abundance studies and other plasma diagnostics.

Subject headings: atomic data — Sun: corona — Sun: UV radiation

1. INTRODUCTION

Transitions within the $n = 2$ complex include forbidden and resonance lines which are important in the study of astrophysical and Tokomak plasmas (Edlen 1983). Such transitions in B-like Mg VIII have been observed from various solar features by the EUV spectrometer-spectroheliosimeter aboard *Skylab* (Vernazza & Reeves 1978), including quiet-Sun, coronal hole, active region, and off-limb. However, interpretation of these *Skylab* observations of Mg VIII had been hampered because of the instruments's low sensitivity below 500 Å and its modest spectral resolution. Much improved observations have recently become available of the same transitions in a similar range of solar features from the Solar EUV Rocket Telescope and Spectrograph (SERTS; Thomas & Neupert 1994; Brosius et al. 1996) and from the Coronal Diagnostic Spectrometer experiment (CDS) on the *Solar and Heliospheric Observatory* (*SOHO*). The line intensities can be used to infer electron densities near the temperature of maximum abundance 8×10^5 K (Arnaud & Rothenflug 1985).

2. ATOMIC DATA

The *Skylab* observations were analyzed by Vernazza & Mason (1978) by interpolating data obtained for other B-like ions. Solar emission lines were also investigated by Dwivedi & Raju (1988). Recently, Zhang & Sampson (1994) calculated collisional data for a number of B-like ions, including Mg VIII, in relativistic distorted wave approximation, but they did not calculate radiative transition rates. For the purpose of analyzing the *SERTS* and *SOHO* observations and any future observations, it was felt necessary to make available radiative and collisional data in one article, obtained consistently using the same target functions.

Atomic data for B-like ions other than Mg VIII have been calculated previously (Bhatia, Feldman, & Seely 1986). That calculation has now been extended to include Mg VIII using

the configurations $2s^22p$, $2s2p^2$, $2p^3$, $2s^23s$, $2s^23p$, $2s^23d$, giving rise to 20 doublet and quartet levels. The wave functions are of configuration-interaction type and are linear combinations of Slater-type orbitals. The radial functions are calculated in the field of a modified Thomas-Fermi potential by using the program Superstructure developed at the University College, London, and described by Eissner, Jones, & Nussbaumer (1974). The scaling parameters (λ_s , λ_p , and λ_d) are found by minimizing the sum of energies. Optimum values are found to be $\lambda_s = 1.3731$, $\lambda_p = 1.1996$, and $\lambda_d = 1.5916$. The spin-orbit interaction, which gives fine structure, and relativistic corrections are treated as a perturbation to the nonrelativistic Hamiltonian. The energy levels, oscillator strengths, and radiative transition rates have been calculated in intermediate coupling.

The energies obtained in this approximation are given in Table 1 and are compared with the observed values given by Martin & Zalubas (1980), Edlen (1983), and Kaufman & Martin (1991). Table 2 lists all coefficients that are greater than 0.01 for the intermediate-coupling wave functions. It is seen that the primary configuration always has the largest coefficient. A comparison of the new dipole-allowed radiative rates for a few transitions of interest with those obtained in multiconfiguration Dirac-Fock technique by Cheng, Kim, & Descleux (1979) is given in Table 3. Their calculation includes Lamb shift of the $1s_{1/2}$, $2s_{1/2}$, and $2p_{1/2}$ electrons in addition to relativistic effects arising from the Dirac Hamiltonian and the Breit operator. The agreement is good. Also given in the same table are the results of the many-body perturbation calculation of Merkelis et al. (1994). A comparison with observations, discussed in § 4, shows that these results are not accurate.

To calculate the excitation cross sections by electron impact, the scattering problem is solved in the distorted approximation by using programs described by Eissner & Seaton (1972). In this approximation, coupling between the channels is neglected. The target wave functions are the same as those obtained from the Superstructure program.

TABLE 1
CALCULATED ENERGY LEVELS OF Mg VIII

KEY	CONFIGURATION	LEVEL	ENERGY (cm ⁻¹)	
			Calculated	Observed
1.....	$2s^2 2p$	$^2P_{1/2}$	0	0
2.....		$^2P_{3/2}$	3273	3302
3.....	$2s 2p^2$	$^4P_{1/2}$	124629	129890
4.....		$^4P_{3/2}$	125777	131030
5.....		$^4P_{5/2}$	127622	132710
6.....		$^2D_{3/2}$	237010	232307
7.....		$^2D_{5/2}$	237051	232274
8.....		$^2S_{1/2}$	301835	298282
9.....		$^2P_{1/2}$	332208	318721
10.....		$^2P_{3/2}$	334355	320723
11.....	$2p^3$	$^4S_{3/2}$	411538	413610
12.....		$^2D_{3/2}$	475625	465818
13.....		$^2D_{5/2}$	475722	465745
14.....		$^2P_{1/2}$	536849	524652
15.....		$^2P_{3/2}$	537104	524841
16.....	$2s^2 3s$	$^2S_{1/2}$	1240331	1210690
17.....	$2s^2 3p$	$^2P_{1/2}$	1307253	...
18.....		$^2P_{3/2}$	1308039	...
19.....	$2s^2 3d$	$^2D_{3/2}$	1364062	1335860
20.....		$^2D_{5/2}$	1364292	1336030

The reactance matrices are calculated in *LS* coupling and, to obtain collision strengths, are transformed to intermediate coupling by using term-coupling coefficients obtained from the Superstructure program in the program JAJOM developed by Saraph (1972). The collision strength Ω (a dimensionless quantity) is defined by

$$\Omega_{ij} = k_i^2 g_i \sigma_{ij},$$

where k_i^2 , g_i , and σ_{ij} are the electron incident energy, weight factor of the lower level i , and excitation cross section from level i to level j , respectively. The scattering calculations were carried out by including intermediate states with total angular momentum L^T , the maximum value being 21. The angular momentum L^T of the intermediate state is defined

by

$$L^T = l_i + l_t,$$

where l_i is the angular momentum of the incident electron and l_t is the angular momentum of the target. In principle, there are an infinite number of incident partial waves, but it is not possible to include all of them. There is an appreciable contribution from higher partial waves for dipole-allowed transitions. Therefore, for higher partial waves ($l_i > L^T - 2$) Coulomb-Bethe contributions (Burgess & Sheorey 1974) have been added. Collision strengths are calculated at five incident energies 15, 22.5, 30, 37.5, and 45 Ry. To check the convergence of collision strength with L^T at the highest energy, collision strengths for randomly chosen dipole-allowed transitions, spin-forbidden forbidden transitions, and spin-allowed forbidden transitions at $L^T = 9, 13, 17$, and 21 are given in Table 4, which shows that they are well converged by $L^T = 21$. Convergence must be better at lower energies, and so such values are not given in Table 4.

The weighted oscillator strengths $g_i f_{ij}$, transition rates A_{ji} , and collision strengths Ω_{ij} at incident energies 15, 22.5, 30, 37.5, and 45 Ry between the 20 levels are tabulated in Table 5. This range of energies is sufficient to calculate rate coefficients at the ambient solar temperature for Mg VIII which is about 8×10^5 K.

Collision strengths for the transitions 1–2, 1–3, and 1–5 are compared in Table 6 with those obtained by Zhang & Sampson (1994) in their relativistic distorted-wave approximation. Collision strengths at 15, 22.5, 30, 37.5, and 45 Ry are obtained by a least-squares fit to their results. The agreement is good, showing that for low nuclear charge Z the relativistic and spin-orbit interaction can be treated as a perturbation to the Hamiltonian. This agreement, in general, holds up to $Z = 26$ (see, e.g., the calculation for Ca XIII by Balyan & Bhatia 1994). The excitation rate coefficients ($\text{cm}^3 \text{s}^{-1}$) are given by

$$C_{ij} = \frac{8.63 \times 10^{-6}}{g_i \sqrt{T_e}} \int_{\Delta E_{ij}}^{\infty} \Omega_{ij} e^{-(E/kT_e)} d(E/kT_e),$$

TABLE 2
Mg VIII LEVEL WAVE FUNCTIONS

Wave Function
$\Phi_{01} = 0.983 C_1 (^2P_{1/2}) - 0.185 C_3 (^2P_{1/2}) + 0.019 C_5 (^2P_{1/2})$
$\Phi_{02} = 0.982 C_1 (^2P_{3/2}) - 0.186 C_3 (^2P_{3/2}) + 0.018 C_5 (^2P_{3/2})$
$\Phi_{03} = 1.000 C_2 (^4P_{1/2}) - 0.015 C_2 (^2S_{1/2})$
$\Phi_{04} = 1.000 C_2 (^4P_{3/2})$
$\Phi_{05} = 1.000 C_2 (^4P_{5/2}) - 0.014 C_2 (^2D_{5/2})$
$\Phi_{06} = 0.999 C_2 (^2D_{3/2}) - 0.034 C_6 (^2D_{3/2}) - 0.015 C_2 (^2P_{3/2})$
$\Phi_{07} = 0.999 C_2 (^2D_{5/2}) - 0.034 C_6 (^2D_{5/2}) + 0.014 C_2 (^4P_{5/2})$
$\Phi_{08} = 0.998 C_2 (^2S_{1/2}) + 0.060 C_2 (^2P_{1/2}) + 0.024 C_4 (^2S_{1/2}) + 0.015 C_2 (^4P_{1/2})$
$\Phi_{09} = 0.998 C_2 (^2P_{1/2}) - 0.060 C_2 (^2S_{1/2})$
$\Phi_{10} = 1.000 C_2 (^2P_{3/2}) + 0.015 C_2 (^2P_{3/2})$
$\Phi_{11} = 1.000 C_3 (^4S_{3/2}) - 0.017 C_2 (^2P_{3/2})$
$\Phi_{12} = 0.999 C_3 (^2D_{3/2}) - 0.039 C_3 (^2P_{3/2})$
$\Phi_{13} = 1.000 C_3 (^2D_{5/2})$
$\Phi_{14} = 0.983 C_3 (^2P_{1/2}) + 0.185 C_1 (^2P_{1/2})$
$\Phi_{15} = 0.982 C_3 (^2P_{3/2}) + 0.186 C_1 (^2P_{3/2}) + 0.040 C_3 (^2D_{3/2})$
$\Phi_{16} = 1.000 C_4 (^2S_{1/2}) - 0.024 C_2 (^2S_{1/2})$
$\Phi_{17} = 1.000 C_5 (^2P_{1/2}) - 0.020 C_1 (^2P_{1/2})$
$\Phi_{18} = 1.000 C_5 (^2P_{3/2}) - 0.019 C_1 (^2P_{3/2})$
$\Phi_{19} = 0.999 C_6 (^2D_{3/2}) + 0.034 C_2 (^2D_{3/2})$
$\Phi_{20} = 0.999 C_6 (^2D_{5/2}) + 0.034 C_2 (^2D_{5/2})$

NOTE.— C_1, C_2, C_3, C_4, C_5 , and C_6 represent $2s^2 2p$, $2s 2p^2$, $2p^3$, $2s^2 3s$, $2s^2 3p$, and $2s^2 3d$, respectively.

TABLE 3
COMPARISON OF CALCULATED TRANSITION RATES A_{ji}

TRANSITION $i-j$	$A_{ji} (\text{s}^{-1})$		
	Present	Cheng et al.	Merkelis et al.
1-6.....	1.534E+9	1.698E+9	3.98E+9
1-8.....	3.483E+9	3.564E+9	3.10E+9
1-9.....	9.878E+9	9.443E+9	4.85E+9
1-10.....	2.620E+9	2.549E+9	1.23E+9
2-7.....	1.720E+9	1.893E+9	7.61E+9
2-8.....	5.046E+9	4.997E+9	2.25E+9
2-9.....	5.899E+9	5.966E+9	2.50E+9
2-10.....	13.27E+9	12.97E+9	6.13E+9

NOTE.—The key to the level numbers in the transition column is given in Table 1.

where k is Boltzmann's constant, T_e is the electron temperature in kelvins and ΔE_{ij} is the energy of the $i \rightarrow j$ transition. The de-excitation rates are given by the principle of detailed balancing. The collision strengths at five energies are fitted to a polynomial to evaluate the above integral.

The level populations are calculated by solving the statistical equilibrium equations

$$N_j \left[\sum_{i < j} A_{ji} + N_e \left(\sum_{i < j} C_{ji}^d + \sum_{i > j} C_{ji}^e \right) \right] = N_e \left(\sum_{i < j} N_i C_{ij}^e + \sum_{i > j} N_i C_{ij}^d \right) + \sum_{i > j} N_i A_{ij},$$

where the superscripts e and d refer to electron excitation and de-excitation, N_j is the number density of level j , and N_e is the electron density.

Proton excitation is important only for transitions between closely lying levels, and therefore we calculated it

TABLE 4
CONVERGENCE OF COLLISION STRENGTHS WITH INCREASING TOTAL ANGULAR MOMENTUM L^T AT INCIDENT ELECTRON ENERGY OF $k^2 = 45$ Ry

TRANSITION $i-j$	COLLISION STRENGTH FOR L^T				
	9	13	17	21	TYPE
1-3.....	4.714E-3	4.722E-3	4.721E-3	4.718E-3	a
1-6.....	1.502E+0	1.497E+0	1.497E+0	1.497E+0	a
2-10.....	4.168E+0	4.154E+0	4.153E+0	4.154E+0	a
3-11.....	1.217E+0	1.214E+0	1.214E+0	1.214E+0	a
6-12.....	3.394E+0	3.387E+0	3.387E+0	3.385E+0	a
10-15.....	5.581E+0	5.572E+0	5.573E+0	5.571E+0	a
1-5.....	3.703E-3	3.709E-3	3.709E-3	3.709E-3	b
1-11.....	1.620E-4	1.620E-4	1.620E-4	1.620E-4	b
2-11.....	3.130E-4	3.140E-4	3.140E-4	3.140E-4	b
3-7.....	6.068E-3	6.074E-3	6.074E-3	6.074E-3	b
5-7.....	3.478E-2	3.483E-2	3.483E-2	3.483E-2	b
11-12.....	2.430E-2	2.432E-2	2.432E-2	2.433E-2	b
1-2.....	8.327E-2	9.442E-2	9.824E-2	9.992E-2	c
1-18.....	6.719E-3	1.303E-2	1.547E-2	1.614E-2	c
4-5.....	1.238E-1	1.393E-1	1.447E-1	1.470E-2	c
6-8.....	1.099E-1	1.291E-1	1.356E-1	1.385E-1	c
7-20.....	5.848E-3	6.071E-3	6.173E-3	6.211E-3	c
12-13.....	5.097E-2	5.106E-2	5.109E-2	5.110E-2	c

NOTE.—The key to the level numbers in the Transition column is given in Table 1.

^a Allowed transitions.

^b Spin-forbidden forbidden transitions.

^c Spin-allowed forbidden transitions.

only between $2s^2 2p(^2P_{1/2}-^2P_{3/2})$ levels by semiclassical approximation (Kastner & Bhatia 1979). The result obtained for the proton excitation-rate coefficient, proportional to the electric quadrupole transition rate A_q , is $0.864 \times 10^{-9} \text{ cm}^3 \text{ s}^{-1}$ at $T_e = 8 \times 10^5 \text{ K}$. Recently, Foster, Keenan, & Reid (1997) have also calculated the above-mentioned coefficient. They get $0.842 \times 10^{-9} \text{ cm}^3 \text{ s}^{-1}$. They have also calculated rate coefficients for transitions $2s2p^2(^4P_{1/2}-^4P_{3/2})$, $^4P_{1/2}-^4P_{5/2}$, $^4P_{3/2}-^4P_{5/2}$, getting 0.116×10^{-9} , 0.604×10^{-9} , and $0.515 \times 10^{-9} \text{ cm}^3 \text{ s}^{-1}$, respectively. We have used their full set of values in our line intensity calculation.

3. LEVEL POPULATIONS

The fractional level populations $n_j = N_j/N_T$ at $T_e = 8.0 \times 10^5 \text{ K}$ and seven electron densities ($\log N_e = 6-12$), are given in Table 7, 8, and 9 for three models. The quantity N_T is the sum of the number densities for 20 levels of Mg VIII included in the calculation. The three models are proton rates and no background radiation included (Table 7); proton rates and blackbody radiation (dilution factor 0.3) included (Table 8); proton rates and background radiation (dilution factor 0.5) included (Table 9). For the background radiation, the dilution factor is defined in Bhatia & Doschek (1995) and the background radiation temperature is 5800 K. Intensity ratios at the above mentioned electron densities can be calculated using

$$I_{ji} = n_j A_{ji} \Delta E_{ji} \text{ (energy units)}.$$

4. COMPARISON WITH OBSERVATIONS

There are eight predicted lines of Mg VIII from $2s^2 2p-2s2p^2$ transitions at EUV wavelengths between 300 and 440 Å. All but one of these are seen in the active region spectrum recorded by SERTS 89 (Thomas & Neupert 1994). Many were also measured in spectra of active regions, quiet-sun, and off-limb observed by SERTS 91 and SERTS 93 (Brosius et al. 1996), as well as in unpublished spectra of active regions from the CDS instrument on SOHO. (CDS itself is described by Harrison et al. 1995.) The quality of these recent spectral observations is demonstrated in Figure 1, which shows five of the Mg VIII lines discussed here. The various measurements have been normalized (in energy units) to the intensity of the strongest line at 315.024 Å and are listed in Tables 10 and 11. Table 12 compares the SERTS 89 observations with calculated intensities (similarly normalized in energy units) at $\log T_e = 5.9$ and at five electron densities ($\log N_e = 6, 7, 8, 9$, and 10). The calculated values include proton excitation and de-excitation rates but no background radiation.

Most of the observations shown in Tables 10–12 agree very well with their corresponding predicted values. Of the few discrepancies, some can be easily explained. For example, the line at 311.78 Å is known to be blended with Ni xv, accounting for the fact that observed active region intensities are greater than would be predicted for Mg VIII alone. The Mg VIII 335.23 Å line is masked by very intense radiation of nearby Fe xvi 335.40 Å for many solar features and so it is not identified separately in these observations; it may become important in spectra of cooler solar plasmas. The measured off-limb intensity of Mg VIII 313.74 Å is significantly larger than predicted, suggesting that in this special case the electron density is of the order of $10^{7.5} \text{ cm}^{-3}$. The effective bandpasses of the analyzed spectra from

TABLE 5
Mg VIII OSCILLATOR STRENGTHS, RADIATIVE DECAY RATES, AND COLLISION STRENGTHS

		COLLISION STRENGTH AT INCIDENT ELECTRON ENERGY (Ry)						
<i>i</i>	<i>j</i>	$g_i f_{ij}$	A_{ji}	15.0	22.5	30.0	37.5	45.0
1.....	2	...	3.151E-01	1.414E-01	1.210E-01	1.103E-01	1.039E-01	9.992E-02
	3	1.415E-05	7.332E+04	1.435E-02	1.011E-02	7.529E-03	5.861E-03	4.718E-03
	4	5.668E-07	1.495E+03	2.040E-02	1.422E-02	1.047E-02	8.041E-03	6.374E-03
	5	1.190E-02	8.292E-03	6.101E-03	4.682E-03	3.709E-03
	6	1.638E-01	1.534E+09	1.154E+00	1.269E+00	1.360E+00	1.434E+00	1.497E+00
	7	2.402E-02	1.665E-02	1.219E-02	9.311E-03	7.356E-03
	8	1.146E-01	3.483E+09	5.702E-01	6.294E-01	6.760E-01	7.144E-01	7.468E-01
	9	2.684E-01	9.878E+09	1.149E+00	1.276E+00	1.376E+00	1.458E+00	1.527E+00
	10	1.405E-01	2.620E+09	6.010E-01	6.653E-01	7.161E-01	7.581E-01	7.936E-01
	11	...	6.763E-01	6.690E-04	4.390E-04	3.030E-04	2.180E-04	1.620E-04
	12	...	4.227E+03	4.341E-03	4.829E-03	5.137E-03	5.353E-03	5.502E-03
	13	...	1.769E+03	3.319E-03	3.406E-03	3.475E-03	3.535E-03	3.580E-03
	14	1.441E-03	1.384E-03	1.354E-03	1.332E-03	1.316E-03
	15	...	3.240E+03	2.163E-03	2.266E-03	2.351E-03	2.414E-03	2.463E-03
	16	3.779E-02	1.939E+10	7.193E-03	8.099E-03	9.655E-03	1.129E-02	1.287E-02
	17	8.253E-02	8.685E-02	8.841E-02	8.918E-02	8.964E-02
	18	...	5.791E+06	2.693E-02	2.063E-02	1.797E-02	1.677E-02	1.614E-02
	19	1.192E+00	3.699E+11	2.610E-01	3.462E-01	4.189E-01	4.814E-01	5.359E-01
	20	5.115E-02	3.187E-02	2.433E-02	2.087E-02	1.906E-02
2.....	3	1.364E-05	6.697E+04	8.923E-03	6.318E-03	4.739E-03	3.719E-03	3.020E-03
	4	5.722E-06	1.432E+04	2.542E-02	1.775E-02	1.311E-02	1.010E-02	8.031E-03
	5	2.636E-05	4.530E+04	5.703E-02	3.994E-02	2.957E-02	2.285E-02	1.824E-02
	6	2.802E-02	2.553E+08	2.315E-01	2.423E-01	2.524E-01	2.617E-01	2.700E-01
	7	2.831E-01	1.720E+09	2.054E+00	2.252E+00	2.409E+00	2.537E+00	2.645E+00
	8	1.697E-01	5.046E+09	8.603E-01	9.480E-01	1.017E+00	1.074E+00	1.123E+00
	9	1.635E-01	5.899E+09	7.164E-01	7.929E-01	8.534E-01	9.033E-01	9.455E-01
	10	7.262E-01	1.327E+10	3.133E+00	3.475E+00	3.745E+00	3.967E+00	4.154E+00
	11	...	3.165E+00	1.294E-03	8.490E-04	5.870E-04	4.210E-04	3.140E-04
	12	...	3.641E+03	4.602E-03	4.767E-03	4.888E-03	4.989E-03	5.062E-03
	13	...	6.056E+03	1.012E-02	1.103E-02	1.161E-02	1.203E-02	1.232E-02
	14	...	7.064E+03	2.412E-03	2.536E-03	2.635E-03	2.709E-03	2.765E-03
	15	...	3.893E+03	5.546E-03	5.581E-03	5.634E-03	5.674E-03	5.705E-03
	16	7.735E-02	3.948E+10	1.438E-02	1.628E-02	1.948E-02	2.282E-02	2.603E-02
	17	...	1.168E+07	2.683E-02	2.063E-02	1.802E-02	1.686E-02	1.625E-02
	18	...	5.840E+06	1.944E-01	1.968E-01	1.972E-01	1.975E-01	1.978E-01
	19	2.393E-01	7.390E+10	1.138E-01	1.079E-01	1.135E-01	1.219E-01	1.307E-01
	20	2.153E+00	4.434E+11	5.126E-01	6.515E-01	7.770E-01	8.872E-01	9.841E-01
3.....	4	...	3.404E-02	1.009E-01	7.037E-02	5.316E-02	4.245E-02	3.530E-02
	5	...	3.826E-07	9.060E-02	8.714E-02	8.586E-02	8.539E-02	8.524E-02
	6	...	1.038E+00	4.001E-02	2.555E-02	1.763E-02	1.286E-02	9.763E-03
	7	...	2.456E-03	2.377E-02	1.540E-02	1.076E-02	7.929E-03	6.074E-03
	8	...	1.128E+01	8.697E-03	5.142E-03	3.323E-03	2.285E-03	1.647E-03
	9	...	4.062E+00	2.832E-03	1.737E-03	1.177E-03	8.550E-04	6.500E-04
	10	...	1.145E+00	6.608E-03	4.165E-03	2.860E-03	2.083E-03	1.584E-03
	11	1.725E-01	2.368E+09	9.214E-01	1.023E+00	1.100E+00	1.162E+00	1.214E+00
	12	2.587E-06	5.314E+04	1.695E-02	1.157E-02	8.373E-03	6.342E-03	4.972E-03
	13	1.862E-03	1.255E-03	9.040E-04	6.830E-04	5.340E-04
	14	1.148E-05	6.504E+05	4.443E-03	2.958E-03	2.112E-03	1.586E-03	1.238E-03
	15	2.495E-07	7.077E+03	2.556E-03	1.684E-03	1.191E-03	8.870E-04	6.860E-04
	16	...	3.876E-02	1.800E-05	8.000E-06	4.000E-06	3.000E-06	2.000E-06
	17	7.142E-07	3.331E+05	1.100E-05	5.000E-06	4.000E-06	3.000E-06	3.000E-06
	18	1.098E-06	2.563E+05	9.000E-06	5.000E-06	4.000E-06	3.000E-06	3.000E-06
	19	...	4.159E+01	1.100E-04	5.300E-05	3.000E-05	2.000E-05	1.400E-05
	20	...	4.064E+01	6.800E-05	3.300E-05	1.900E-05	1.300E-05	9.000E-06
4.....	5	...	1.016E-01	2.243E-01	1.871E-01	1.670E-01	1.549E-01	1.470E-01
	6	...	3.959E+00	6.214E-02	3.978E-02	2.752E-02	2.010E-02	1.528E-02
	7	...	2.114E+00	6.568E-02	4.229E-02	2.940E-02	2.156E-02	1.646E-02
	8	...	5.193E+01	1.708E-02	1.010E-02	6.530E-03	4.491E-03	3.238E-03
	9	...	1.974E-01	6.259E-03	3.887E-03	2.649E-03	1.926E-03	1.464E-03
	10	...	2.527E+00	1.341E-02	8.410E-03	5.758E-03	4.188E-03	3.183E-03
	11	3.437E-01	4.680E+09	1.843E+00	2.048E+00	2.202E+00	2.327E+00	2.431E+00
	12	3.948E-05	8.057E+05	2.260E-02	1.547E-02	1.125E-02	8.569E-03	6.764E-03
	13	5.774E-06	7.860E+04	1.476E-02	1.006E-02	7.279E-03	5.514E-03	4.326E-03
	14	2.229E-06	1.256E+05	6.753E-03	4.477E-03	3.177E-03	2.374E-03	1.842E-03
5.....	15	4.532E-05	1.279E+06	8.021E-03	5.360E-03	3.852E-03	2.923E-03	2.312E-03
	16	...	1.244E+01	3.600E-05	1.600E-05	8.000E-06	5.000E-06	3.000E-06
	17	1.710E-07	7.961E+04	1.500E-05	6.000E-06	4.000E-06	3.000E-06	2.000E-06
	18	1.498E-10	3.492E+01	1.800E-05	7.000E-06	4.000E-06	3.000E-06	2.000E-06
	19	...	3.440E+00	1.730E-04	8.400E-05	4.800E-05	3.100E-05	2.200E-05
5.....	20	...	7.413E-01	1.830E-04	8.900E-05	5.100E-05	3.300E-05	2.400E-05
	6	...	1.180E+00	5.120E-02	3.314E-02	2.314E-02	1.703E-02	1.304E-02

TABLE 5—Continued

COLLISION STRENGTH AT INCIDENT ELECTRON ENERGY (Ry)								
<i>i</i>	<i>j</i>	$g_i f_{ij}$	A_{ji}	15.0	22.5	30.0	37.5	45.0
6	7	...	1.029E+01	1.412E-01	9.044E-02	6.261E-02	4.577E-02	3.483E-02
	8	...	5.814E-02	2.489E-02	1.474E-02	9.532E-03	6.560E-03	4.732E-03
	9	...	1.743E-02	1.163E-02	7.326E-03	5.024E-03	3.652E-03	2.771E-03
	10	...	3.196E+00	1.975E-02	1.227E-02	8.355E-03	6.065E-03	4.604E-03
	11	5.122E-01	6.885E+09	2.768E+00	3.077E+00	3.311E+00	3.499E+00	3.656E+00
	12	8.641E-06	1.745E+05	4.509E-03	3.069E-03	2.228E-03	1.696E-03	1.339E-03
	13	1.827E-04	2.461E+06	5.081E-02	3.496E-02	2.557E-02	1.962E-02	1.561E-02
	14	...	3.947E-03	2.604E-03	1.844E-03	1.374E-03	1.064E-03	
	15	1.870E-05	5.228E+05	1.978E-02	1.313E-02	9.331E-03	6.980E-03	5.427E-03
	16	...	1.172E+02	5.400E-05	2.400E-05	1.200E-05	7.000E-06	5.000E-06
	17	...	9.000E-06	4.000E-06	2.000E-06	2.000E-06	1.000E-06	
	18	1.413E-06	3.284E+05	4.200E-05	1.800E-05	1.300E-05	1.000E-05	8.000E-06
	19	...	8.559E+00	1.440E-04	7.000E-05	4.100E-05	2.700E-05	1.900E-05
	20	...	2.285E+01	3.920E-04	1.890E-04	1.090E-04	7.100E-05	5.100E-05
7	7	...	7.302E-07	1.209E-01	1.057E-01	9.620E-02	9.271E-02	8.896E-02
	8	...	9.602E+00	1.156E-01	1.244E-01	1.307E-01	1.352E-01	1.385E-01
	9	...	3.401E+00	2.174E-02	1.395E-02	9.732E-03	7.198E-03	5.558E-03
	10	...	5.819E+00	6.075E-02	3.845E-02	2.642E-02	1.923E-02	1.460E-02
	11	1.163E-08	5.907E+01	7.000E-05	3.100E-05	1.600E-05	1.000E-05	6.000E-06
	12	3.723E-01	3.535E+09	2.568E+00	2.865E+00	3.078E+00	3.246E+00	3.385E+00
	13	4.810E-02	3.047E+08	3.705E-01	3.955E-01	4.154E-01	4.324E-01	4.474E-01
	14	2.347E-01	7.037E+09	1.158E+00	1.302E+00	1.407E+00	1.490E+00	1.558E+00
	15	5.272E-02	7.917E+08	2.689E-01	2.979E-01	3.197E-01	3.371E-01	3.517E-01
	16	...	2.702E+05	5.200E-04	6.330E-04	7.150E-04	7.650E-04	7.890E-04
	17	4.120E-03	1.574E+09	3.120E-04	5.340E-04	7.770E-04	1.007E-03	1.222E-03
	18	8.973E-04	1.716E+08	2.780E-04	3.210E-04	3.780E-04	4.230E-04	4.660E-04
	19	...	8.112E+04	3.889E-03	3.945E-03	4.014E-03	4.046E-03	4.090E-03
	20	...	2.320E+04	3.230E-04	1.920E-04	1.640E-04	1.570E-04	1.540E-04
8	8	...	1.434E+01	1.731E-01	1.864E-01	1.958E-01	2.026E-01	2.076E-01
	9	...	3.527E-01	4.714E-02	3.004E-02	2.084E-02	1.535E-02	1.181E-02
	10	...	3.308E+00	7.622E-02	4.833E-02	3.325E-02	2.422E-02	1.839E-02
	11	1.173E-06	5.954E+03	9.500E-05	4.700E-05	3.000E-05	2.400E-05	2.100E-05
	12	5.317E-02	5.047E+08	4.009E-01	4.322E-01	4.564E-01	4.765E-01	4.938E-01
	13	6.020E-01	3.812E+09	4.166E+00	4.640E+00	4.982E+00	5.251E+00	5.476E+00
	14	7.677E-03	4.954E-03	3.480E-03	2.585E-03	2.000E-03
	15	4.016E-01	6.029E+09	1.981E+00	2.227E+00	2.406E+00	2.548E+00	2.664E+00
	16	...	4.052E+05	7.800E-04	9.490E-04	1.073E-03	1.148E-03	1.184E-03
	17	1.720E-04	1.650E-04	1.670E-04	1.670E-04	1.660E-04
	18	7.789E-03	1.490E+09	7.070E-04	1.124E-03	1.583E-03	2.021E-03	2.421E-03
	19	...	3.474E+04	3.240E-04	1.920E-04	1.640E-04	1.570E-04	1.540E-04
	20	...	9.276E+04	5.992E-03	6.012E-03	6.100E-03	6.145E-03	6.211E-03
9	9	...	3.596E+00	9.596E-03	5.613E-03	3.608E-03	2.476E-03	1.780E-03
	10	...	1.111E+00	1.836E-02	1.078E-02	6.970E-03	4.822E-03	3.503E-03
	11	3.906E-07	7.838E+02	1.100E-04	8.000E-05	6.100E-05	5.000E-05	4.200E-05
	12	1.899E-03	9.566E+06	2.063E-02	2.274E-02	2.428E-02	2.549E-02	2.650E-02
	13	7.200E-05	2.800E-05	1.500E-05	9.000E-06	6.000E-06
	14	5.410E-02	9.965E+08	3.887E-01	4.313E-01	4.619E-01	4.859E-01	5.059E-01
	15	1.493E-01	1.378E+09	1.069E+00	1.187E+00	1.271E+00	1.337E+00	1.392E+00
	16	...	3.278E-04	1.397E-03	1.523E-03	1.574E-03	1.597E-03	1.611E-03
	17	3.406E-03	1.148E+09	5.380E-04	8.660E-04	1.130E-03	1.363E-03	1.571E-03
	18	6.236E-03	1.053E+09	9.540E-04	1.542E-03	2.030E-03	2.455E-03	2.833E-03
	19	...	1.175E+05	3.700E-04	4.680E-04	5.400E-04	5.890E-04	6.150E-04
	20	...	1.177E+05	5.490E-04	6.980E-04	8.080E-04	8.820E-04	9.220E-04
10.....	10	...	8.869E-02	1.412E-01	1.214E-01	1.120E-01	1.069E-01	1.039E-01
	11	1.009E-05	1.059E+04	1.561E-02	1.063E-02	7.752E-03	5.947E-03	4.744E-03
	12	2.237E-01	7.674E+08	3.167E+00	3.479E+00	3.703E+00	3.880E+00	4.028E+00
	13	4.010E-03	2.665E-03	1.904E-03	1.425E-03	1.108E-03
	14	2.028E-01	2.832E+09	1.741E+00	1.942E+00	2.081E+00	2.190E+00	2.279E+00
	15	7.054E-02	4.939E+08	6.062E-01	6.760E-01	7.242E-01	7.617E-01	7.925E-01
	16	...	6.355E-02	2.400E-05	1.400E-05	1.000E-05	9.000E-06	8.000E-06
	17	3.950E-04	1.252E+08	2.760E-04	3.430E-04	3.930E-04	4.290E-04	4.570E-04
	18	4.141E-04	6.576E+07	2.040E-04	2.640E-04	3.080E-04	3.400E-04	3.670E-04
	19	...	3.883E+02	5.400E-05	2.400E-05	1.500E-05	1.100E-05	9.000E-06
	20	...	3.855E+02	8.000E-05	4.600E-05	3.100E-05	2.300E-05	1.800E-05
	11	4.276E-05	4.248E+04	3.168E-02	2.190E-02	1.626E-02	1.271E-02	1.036E-02
	12	3.590E-02	1.195E+08	5.270E-01	5.746E-01	6.095E-01	6.374E-01	6.609E-01
	13	3.795E-01	8.432E+08	5.488E+00	6.024E+00	6.409E+00	6.713E+00	6.967E+00
	14	9.069E-02	1.240E+09	7.930E-01	8.831E-01	9.456E-01	9.943E-01	1.034E+00
	15	4.897E-01	3.357E+09	4.256E+00	4.747E+00	5.087E+00	5.352E+00	5.571E+00
	16	...	4.287E+01	3.700E-05	1.600E-05	8.000E-06	5.000E-06	3.000E-06
	17	3.076E-04	9.710E+07	1.760E-04	2.200E-04	2.530E-04	2.770E-04	2.960E-04
	18	1.170E-03	1.850E+08	7.310E-04	9.310E-04	1.065E-03	1.172E-03	1.264E-03

TABLE 5—Continued

		COLLISION STRENGTH AT INCIDENT ELECTRON ENERGY (Ry)						
<i>i</i>	<i>j</i>	$g_i f_{ij}$	A_{ji}	15.0	22.5	30.0	37.5	45.0
11.....	19	...	1.511E+01	1.030E-04	5.600E-05	3.700E-05	2.700E-05	2.000E-05
	20	...	4.141E+00	1.600E-04	7.500E-05	4.700E-05	3.300E-05	2.400E-05
	12	...	4.223E-02	1.048E-01	6.514E-02	4.436E-02	3.212E-02	2.433E-02
	13	...	2.340E-03	1.570E-01	9.766E-02	6.652E-02	4.819E-02	3.650E-02
	14	...	1.084E+01	3.060E-02	1.725E-02	1.082E-02	7.284E-03	5.162E-03
	15	...	2.706E+01	6.110E-02	3.447E-02	2.163E-02	1.457E-02	1.033E-02
	16	1.453E-06	3.329E+05	4.000E-06	5.000E-06	5.000E-06	5.000E-06	6.000E-06
	17	...	2.874E+01	1.000E-06	1.000E-06	1.000E-06
	18	...	1.442E+01	4.000E-06	4.000E-06	4.000E-06	4.000E-06	4.000E-06
	19	3.518E-06	5.322E+05	1.000E-05	1.100E-05	1.100E-05	1.200E-05	1.300E-05
12.....	20	3.267E-05	3.297E+06	2.700E-05	2.900E-05	3.300E-05	3.700E-05	3.800E-05
	13	...	9.986E-06	2.115E-01	1.326E-01	9.120E-02	6.678E-02	5.110E-02
	14	...	7.903E+00	1.325E-01	1.384E-01	1.438E-01	1.481E-01	1.514E-01
	15	...	1.066E+01	1.637E-01	1.558E-01	1.547E-01	1.554E-01	1.565E-01
	16	5.599E-06	1.092E+06	1.300E-05	1.400E-05	1.300E-05	1.400E-05	1.300E-05
	17	...	1.463E+01	1.900E-05	7.000E-06	3.000E-06	1.000E-06	1.000E-06
	18	...	8.597E+01	4.500E-05	2.500E-05	1.900E-05	1.700E-05	1.600E-05
	19	1.357E-03	1.785E+08	1.174E-03	1.337E-03	1.484E-03	1.625E-03	1.744E-03
	20	6.043E-04	5.305E+07	5.330E-04	5.630E-04	6.160E-04	6.680E-04	7.170E-04
	14	...	5.247E+00	1.147E-01	1.072E-01	1.054E-01	1.053E-01	1.057E-01
13.....	15	...	9.353E+00	3.306E-01	3.352E-01	3.435E-01	3.511E-01	3.574E-01
	16	...	2.000E-06
	17	...	1.527E+01	2.100E-05	7.000E-06	3.000E-06	1.000E-06	1.000E-06
	18	...	2.362E+01	4.700E-05	1.500E-05	6.000E-06	3.000E-06	2.000E-06
	19	1.806E-04	2.376E+07	2.770E-04	2.320E-04	2.300E-04	2.380E-04	2.430E-04
	20	2.555E-03	2.243E+08	2.147E-03	2.456E-03	2.741E-03	3.006E-03	3.229E-03
	15	...	1.479E-04	8.624E-02	5.388E-02	3.713E-02	2.730E-02	2.101E-02
	16	1.325E-03	2.187E+08	8.770E-04	1.091E-03	1.303E-03	1.484E-03	1.635E-03
	17	3.159E-03	3.124E-03	3.063E-03	3.016E-03	2.980E-03
	18	...	1.128E+04	1.196E-03	8.590E-04	6.990E-04	6.190E-04	5.700E-04
14.....	19	3.114E-02	3.553E+09	2.056E-02	2.610E-02	3.063E-02	3.444E-02	3.768E-02
	20	2.812E-03	1.439E-03	9.680E-04	7.670E-04	6.680E-04
	16	2.754E-03	4.541E+08	1.759E-03	2.216E-03	2.656E-03	3.031E-03	3.346E-03
	17	...	2.373E+04	1.205E-03	8.710E-04	7.130E-04	6.350E-04	5.860E-04
	18	...	1.184E+04	7.749E-03	7.338E-03	7.051E-03	6.874E-03	6.748E-03
	19	6.606E-03	7.533E+08	7.744E-03	7.264E-03	7.655E-03	8.219E-03	8.784E-03
	20	5.686E-02	4.325E+09	3.959E-02	4.859E-02	5.645E-02	6.320E-02	6.901E-02
	17	2.797E-01	4.178E+08	9.973E+00	1.049E+01	1.077E+01	1.105E+01	1.132E+01
	18	5.659E-01	4.326E+08	1.986E+01	2.089E+01	2.146E+01	2.202E+01	2.254E+01
	19	...	2.518E+03	5.623E-01	5.546E-01	5.428E-01	5.296E-01	5.153E-01
15.....	20	...	2.541E+03	8.435E-01	8.320E-01	8.141E-01	7.944E-01	7.729E-01
	18	...	4.361E-03	9.174E-01	8.216E-01	7.836E-01	7.541E-01	7.270E-01
	19	3.509E-01	1.888E+08	1.602E+01	1.655E+01	1.693E+01	1.734E+01	1.773E+01
	20	1.725E-01	1.301E-01	1.265E-01	1.275E-01	1.285E-01
16.....	19	6.915E-02	3.619E+07	3.425E+00	3.480E+00	3.550E+00	3.633E+00	3.712E+00
	20	6.249E-01	2.198E+08	2.906E+01	2.998E+01	3.065E+01	3.139E+01	3.209E+01
	19	20	...	1.311E-04	7.629E-01	4.214E-01	3.514E-01	3.287E-01

SERTS 91/93 and CDS did not include wavelengths between 430 and 440 Å, so the last two Mg VIII lines could not have been measured by them.

On the other hand, the intensity of Mg VIII 430.44 Å observed by SERTS 89 is outside the calculated range, while the observed intensity of the 436.73 Å line implies an

electron density less than 10^8 cm^{-3} , which is too low for a solar active region. To analyze this discrepancy, it is seen that the calculated intensity ratio $I(313.74)/I(317.01) = 1.69$ agrees well with most of the various observations. This ratio is independent of upper level population, indicating that the transition rates are reliable. As a check, another calculation

TABLE 6
COMPARISON OF COLLISION STRENGTHS WITH ZHANG & SAMPSON RESULTS

<i>E</i> (Ry)	TRANSITION 1-2		TRANSITION 1-3		TRANSITION 1-5	
	PC ^a	ZS ^b	PC ^a	ZS ^b	PC ^a	ZS ^b
15.0.....	1.41E-1	1.49E-1	1.44E-2	1.39E-2	1.19E-2	1.21E-2
22.5.....	1.21E-1	1.22E-1	1.01E-2	9.80E-3	8.29E-3	8.50E-3
30.0.....	1.10E-1	1.04E-1	7.53E-3	7.43E-3	6.10E-3	6.00E-3
37.5.....	1.04E-1	9.60E-2	5.86E-3	6.26E-3	4.68E-3	4.20E-3
45.0.....	9.99E-2	9.40E-2	4.72E-3	5.17E-3	3.71E-3	3.20E-3

^a PC denotes presently calculated collision strengths.

^b ZS denotes collision strengths calculated by Zhang & Sampson.

TABLE 7
Mg VIII FRACTIONAL LEVEL POPULATIONS: WITH PROTON EXCITATION RATES

KEY	POPULATION AT $\log N_e$						
	6	7	8	9	10	11	12
1	9.83E-01	8.62E-01	5.17E-01	3.57E-01	3.35E-01	3.33E-01	3.30E-01
2	1.70E-02	1.38E-01	4.83E-01	6.43E-01	6.65E-01	6.66E-01	6.61E-01
3	6.51E-10	5.97E-09	4.41E-08	3.69E-07	3.60E-06	3.62E-05	3.92E-04
4	8.36E-09	7.98E-08	6.91E-07	6.41E-06	6.33E-05	6.21E-04	5.29E-03
5	1.76E-09	2.05E-08	2.87E-07	3.25E-06	3.31E-05	3.32E-04	3.33E-03
6	1.74E-12	1.55E-11	1.01E-10	7.61E-10	7.27E-09	7.23E-08	7.18E-07
7	1.05E-13	2.97E-12	8.41E-11	1.09E-09	1.13E-08	1.13E-07	1.12E-06
8	1.63E-13	1.59E-12	1.45E-11	1.39E-10	1.38E-09	1.38E-08	1.37E-07
9	1.65E-13	1.51E-12	1.12E-11	9.35E-11	9.10E-10	9.07E-09	9.00E-08
10.....	8.94E-14	1.06E-12	1.55E-11	1.77E-10	1.80E-09	1.80E-08	1.79E-07
11.....	1.69E-16	1.68E-15	1.68E-14	1.69E-13	1.83E-12	3.25E-11	1.61E-09
12.....	1.54E-15	1.46E-14	1.25E-13	1.15E-12	1.14E-11	1.14E-10	1.18E-09
13.....	1.35E-15	1.41E-14	1.59E-13	1.68E-12	1.69E-11	1.70E-10	1.75E-09
14.....	3.14E-16	2.99E-15	2.58E-14	2.39E-13	2.37E-12	2.37E-11	2.41E-10
15.....	3.63E-16	3.84E-15	4.45E-14	4.73E-13	4.77E-12	4.78E-11	4.86E-10
16.....	1.72E-16	1.73E-15	1.74E-14	1.75E-13	1.75E-12	1.75E-11	1.73E-10
17.....	1.13E-14	1.01E-13	6.81E-13	5.25E-12	5.04E-11	5.01E-10	4.97E-09
18.....	3.69E-15	4.88E-14	8.27E-13	9.84E-12	1.01E-10	1.01E-09	9.99E-09
19.....	2.67E-16	2.40E-15	1.65E-14	1.31E-13	1.26E-12	1.25E-11	1.24E-10
20.....	4.69E-17	7.36E-16	1.49E-14	1.84E-13	1.89E-12	1.89E-11	1.88E-10

has been carried out by including three more configurations $2s2p3s$, $2s2p3p$, and $2s2p3d$ to the above six configurations. The transition rates changed by less than 1%.

Although the observed intensities of these lines relative to 315.02 Å are smaller than calculated, their intensities relative to one another fall well within the predicted range. Since the pair is relatively close in wavelength while somewhat separated from the other Mg VIII lines, another possibility is that the present calculations are correct, but that the radiometric calibration of SERTS 89 data may need some adjustment in the region above 400 Å. The situation would be remedied if the instrumental sensitivity were reduced from its nominal value at 410 Å down to a factor of 2.0 less at wavelengths of 430 Å and longward, which is

precisely the result suggested by an extensive analysis of SERTS 89 density-insensitive ratios made by Young, Landi, & Thomas (1998). Yet other studies of line ratios from the SERTS 89 spectrum indicate that the published instrumental sensitivity at these wavelengths relative to shorter wavelengths is either correct (Keenan et al. 1993, 1994) or else perhaps as much as a factor of 4 too low already (Brickhouse, Raymond, & Smith 1995). In any case, no instrumental change will bring all of these various results into agreement, and so the possibility of calibration error must still be considered unresolved.

If the radiative rates calculated by Merkelis et al. (1994) and given in Table 3 are used in place of the presently calculated ones, the predicted intensities of lines at 430.44

TABLE 8
Mg VIII FRACTIONAL LEVEL POPULATIONS: WITH PROTON EXCITATION RATES AND SOLAR BLACKBODY RADIATION EXCITATION (DILUTION FACTOR = 0.3)

KEY	POPULATION AT $\log N_e$						
	6	7	8	9	10	11	12
1	7.14E-01	6.69E-01	4.86E-01	3.57E-01	3.35E-01	3.33E-01	3.30E-01
2	2.86E-01	3.31E-01	5.14E-01	6.43E-01	6.65E-01	6.66E-01	6.61E-01
3	5.30E-10	5.10E-09	4.28E-08	3.69E-07	3.60E-06	3.62E-05	3.92E-04
4	7.53E-09	7.39E-08	6.82E-07	6.41E-06	6.33E-05	6.21E-04	5.29E-03
5	2.41E-09	2.51E-08	2.94E-07	3.25E-06	3.31E-05	3.32E-04	3.33E-03
6	1.32E-12	1.25E-11	9.64E-11	7.61E-10	7.27E-09	7.23E-08	7.18E-07
7	5.29E-13	6.01E-12	8.90E-11	1.09E-09	1.13E-08	1.13E-07	1.12E-06
8	1.53E-13	1.51E-12	1.44E-11	1.39E-10	1.38E-09	1.38E-08	1.37E-07
9	1.34E-13	1.29E-12	1.08E-11	9.35E-11	9.10E-10	9.07E-09	9.00E-08
10.....	1.27E-13	1.33E-12	1.59E-11	1.77E-10	1.80E-09	1.80E-08	1.79E-07
11.....	1.68E-16	1.68E-15	1.67E-14	1.69E-13	1.83E-12	3.25E-11	1.61E-09
12.....	1.37E-15	1.34E-14	1.23E-13	1.15E-12	1.14E-11	1.14E-10	1.18E-09
13.....	1.49E-15	1.51E-14	1.61E-13	1.68E-12	1.69E-11	1.70E-10	1.75E-09
14.....	2.82E-16	2.76E-15	2.55E-14	2.39E-13	2.37E-12	2.37E-11	2.41E-10
15.....	4.10E-16	4.18E-15	4.50E-14	4.73E-13	4.77E-12	4.78E-11	4.86E-10
16.....	1.73E-16	1.74E-15	1.74E-14	1.75E-13	1.75E-12	1.75E-11	1.73E-10
17.....	8.72E-15	8.28E-14	6.51E-13	5.25E-12	5.04E-11	5.01E-10	4.97E-09
18.....	6.33E-15	6.77E-14	8.57E-13	9.84E-12	1.01E-10	1.01E-09	9.99E-09
19.....	2.08E-16	1.98E-15	1.59E-14	1.31E-13	1.26E-12	1.25E-11	1.24E-10
20.....	1.06E-16	1.16E-15	1.56E-14	1.84E-13	1.89E-12	1.89E-11	1.88E-10

TABLE 9

Mg VIII FRACTIONAL LEVEL POPULATIONS: WITH PROTON EXCITATION RATES AND SOLAR BLACKBODY RADIATION EXCITATION (DILUTION FACTOR = 0.5)

KEY	POPULATION AT $\log N_e$						
	6	7	8	9	10	11	12
1	6.32E-01	6.04E-01	4.71E-01	3.56E-01	3.35E-01	3.33E-01	3.30E-01
2	3.68E-01	3.96E-01	5.29E-01	6.44E-01	6.65E-01	6.66E-01	6.61E-01
3	4.93E-10	4.80E-09	4.21E-08	3.69E-07	3.60E-06	3.62E-05	3.92E-04
4	7.27E-09	7.18E-08	6.77E-07	6.41E-06	6.33E-05	6.21E-04	5.29E-03
5	2.60E-09	2.67E-08	2.98E-07	3.26E-06	3.31E-05	3.32E-04	3.33E-03
6	1.19E-12	1.15E-11	9.40E-11	7.60E-10	7.27E-09	7.23E-08	7.18E-07
7	6.60E-13	7.05E-12	9.14E-11	1.10E-09	1.13E-08	1.13E-07	1.12E-06
8	1.50E-13	1.49E-12	1.44E-11	1.39E-10	1.38E-09	1.38E-08	1.37E-07
9	1.25E-13	1.22E-12	1.07E-11	9.34E-11	9.10E-10	9.07E-09	9.00E-08
10.....	1.39E-13	1.43E-12	1.61E-11	1.77E-10	1.80E-09	1.80E-08	1.79E-07
11.....	1.68E-16	1.68E-15	1.67E-14	1.69E-13	1.83E-12	3.25E-11	1.61E-09
12.....	1.32E-15	1.30E-14	1.22E-13	1.15E-12	1.14E-11	1.14E-10	1.18E-09
13.....	1.53E-15	1.55E-14	1.62E-13	1.68E-12	1.69E-11	1.70E-10	1.75E-09
14.....	2.72E-16	2.69E-15	2.53E-14	2.39E-13	2.37E-12	2.37E-11	2.41E-10
15.....	4.24E-16	4.29E-15	4.53E-14	4.73E-13	4.77E-12	4.78E-11	4.86E-10
16.....	1.74E-16	1.74E-15	1.74E-14	1.75E-13	1.75E-12	1.75E-11	1.73E-10
17.....	7.92E-15	7.64E-14	6.36E-13	5.24E-12	5.04E-11	5.01E-10	4.97E-09
18.....	7.14E-15	7.42E-14	8.72E-13	9.85E-12	1.01E-10	1.01E-09	9.99E-09
19.....	1.90E-16	1.84E-15	1.55E-14	1.30E-13	1.26E-12	1.25E-11	1.24E-10
20.....	1.24E-16	1.30E-15	1.59E-14	1.84E-13	1.89E-12	1.89E-11	1.88E-10

and 436.73 Å at $N_e = 10^9 \text{ cm}^{-3}$ become 0.977 and 2.816 relative to 315.02 Å, making the comparison with observations even worse. In addition, $I(313.74)/I(317.01)$ becomes 1.96, also further removed from the observed values, indicating that the radiative rates of Merkleis et al. are not as accurate as those presented here.

The intensity ratio $I(436.73)/I(430.44)$ is found to be density sensitive as shown in Table 12. At $\log N_e = 9.2$

(interpolated), its value is 1.68, which is the observed value from SERTS 89 (Thomas & Neupert 1994). This density is comparable to the value of $\log N_e = 9.6$ derived by Brickhouse et al. (1995) from the same SERTS 89 spectrum but using Fe IX line ratios formed at similar temperatures to those of Mg VIII. The agreement gives some added support to the accuracy of both sets of calculations.

Another atomic database recently made available is

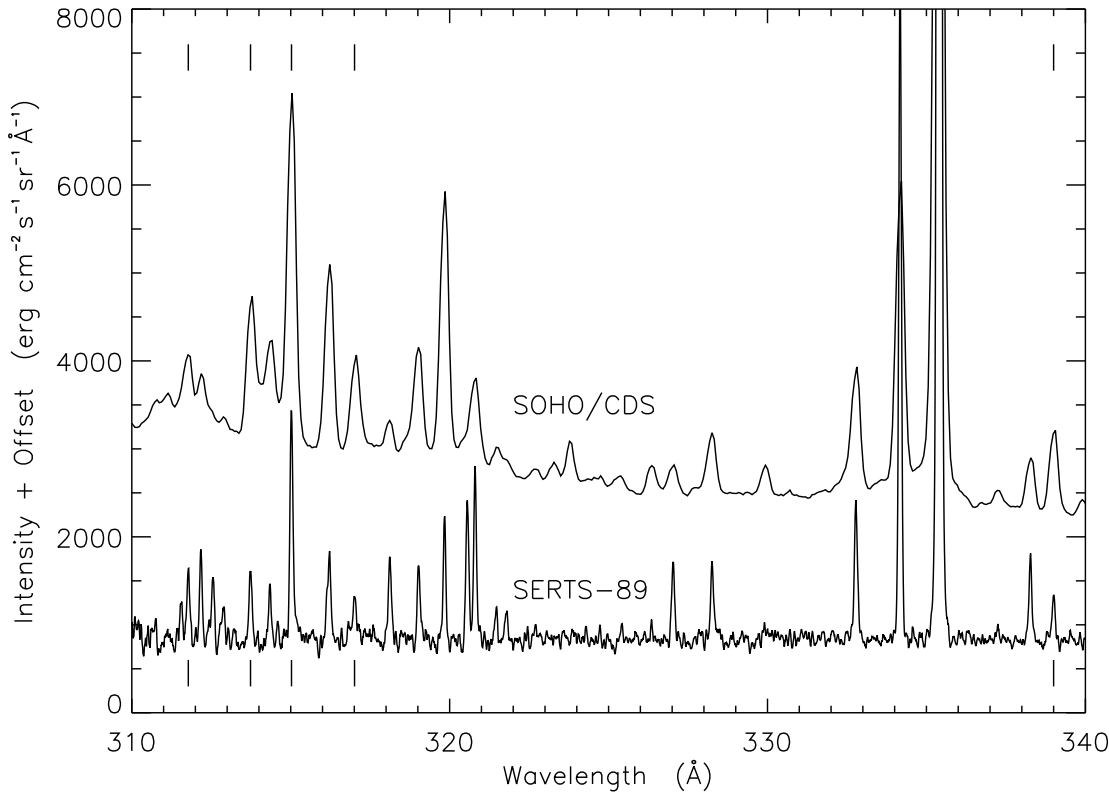


FIG. 1.—Comparison of average active region spectra taken at different times by SERTS 89 and by CDS on SOHO. The tick marks indicate Mg VIII lines analyzed in this paper.

TABLE 10
RELATIVE Mg VIII INTENSITIES OF SOLAR ACTIVE REGIONS OBSERVED BY
SERTS AND BY *SOHO/CDS*

λ (Å)	<i>SERTS</i>			<i>SOHO/CDS</i> 1996
	1989 ^a	1991 ^b	1993 ^b	
311.78 ^c	0.31 ± 0.06	...	0.17 ± 0.03	0.29 ± 0.02
313.74	0.32 ± 0.05	0.29 ± 0.07	0.29 ± 0.05	0.37 ± 0.01
315.02	1.00 ± 0.12 ^d	1.00 ± 0.14 ^e	1.00 ± 0.12 ^f	1.00 ± 0.03 ^g
317.01	0.23 ± 0.05	0.33 ± 0.06	0.24 ± 0.04	0.25 ± 0.01
339.00	0.21 ± 0.03	0.19 ± 0.08	0.28 ± 0.05	0.22 ± 0.01
430.44	0.16 ± 0.02
436.73	0.27 ± 0.03

^a Thomas & Neupert 1994.^b Brosius et al. 1996.^c Blended with Ni xv in active regions.^d Observed intensity is 314 ± 38 ergs $\text{cm}^{-2} \text{s}^{-1} \text{sr}^{-1}$.^e Observed intensity is 80 ± 11 ergs $\text{cm}^{-2} \text{s}^{-1} \text{sr}^{-1}$.^f Observed intensity is 232 ± 27 ergs $\text{cm}^{-2} \text{s}^{-1} \text{sr}^{-1}$.^g Observed intensity is 1370 ± 38 ergs $\text{cm}^{-2} \text{s}^{-1} \text{sr}^{-1}$.

TABLE 11

RELATIVE Mg VIII INTENSITIES OF SOLAR QUIET REGIONS
OBSERVED BY *SERTS*^a

λ (Å)	QUIET DISK		OFF-LIMB 1991
	1991	1993	
311.78.....	...	0.30 ± 0.07	...
313.74.....	...	0.29 ± 0.05	0.82 ± 0.14
315.02.....	1.00 ± 0.13 ^b	1.00 ± 0.12 ^c	1.00 ± 0.17 ^d
317.01.....	0.17 ± 0.05	0.29 ± 0.04	0.40 ± 0.10
339.00.....	0.15 ± 0.04	0.16 ± 0.03	...

^a Brosius et al. 1996.^b Observed intensity is 114.0 ± 14.7 ergs $\text{cm}^{-2} \text{s}^{-1} \text{sr}^{-1}$.^c Observed intensity is 43.9 ± 5.2 ergs $\text{cm}^{-2} \text{s}^{-1} \text{sr}^{-1}$.^d Observed intensity is 88.1 ± 14.6 ergs $\text{cm}^{-2} \text{s}^{-1} \text{sr}^{-1}$.

Chianti (Dere et al. 1997). Over the full density range of 10^6 – 10^{12} , our present results agree within 20% with those of Chianti. However, it should be pointed out that Chianti data do not include proton excitation rates.

In conclusion, consistently calculated atomic data for Mg VIII are presented. The calculated intensities of various lines agree well with observations, both from *SERTS* and from *SOHO*. There are still discrepancies for 430.44 and 436.73 Å lines, and we encourage *R*-matrix calculations, which include contribution due to resonances, for this ion.

This work was supported by RTOP grants 344-12-53-14 and 344-17-38-01 from the Solar Physics Office of NASA's Space Physics Division.

TABLE 12
RELATIVE Mg VIII INTENSITIES: OBSERVED VERSUS CALCULATED

TRANSITION $i-j$	λ (Å)	I_{obs} ^a	$I_{\text{cal}} (\log T_e = 5.9) \text{ AT } \log N_e$				
			6	7	8	9	10 ^b
1–10	311.78	0.31 ± 0.06 ^c	0.199	0.199	0.199	0.199	0.199
1–9	313.74	0.32 ± 0.05	1.380	1.062	0.540	0.395	0.378
2–10	315.02	1.00 ± 0.12	1.000	1.000	1.000	1.000	1.000
2–9	317.01	0.23 ± 0.05	0.816	0.628	0.319	0.233	0.223
1–8	335.23	^d	0.437	0.357	0.225	0.188	0.184
2–8	339.00	0.21 ± 0.03	0.627	0.511	0.322	0.269	0.263
1–6	430.44	0.16 ± 0.02	1.614	1.208	0.542	0.356	0.334
2–7	436.73	0.27 ± 0.03	0.108	0.255	0.498	0.566	0.574

^a SERTS 89 Active Region (Thomas & Neupert 1994).^b Above $\log N_e = 10$, values do not change.^c Blended with Ni xv in active regions.^d Masked by Fe xvi 335.40 Å in active regions.

REFERENCES

- Arnaud, M., & Rothenflug, R. 1985, A&AS, 60, 425
 Baliyan, K. S., & Bhatia, A. K. 1994, J. Phys. B, 27, 4281
 Bhatia, A. K., & Doschek, G. A. 1995, Atom. Data Nucl. Data Tables, 60, 97
 Bhatia, A. K., Feldman, U., & Seely, J. F. 1986, Atom. Data Nucl. Data Tables, 35, 319
 Brickhouse, N. S., Raymond, J. C., & Smith, B. W. 1995, ApJS, 97, 551
 Brosius, J. W., Davila, J. M., Thomas, R. J., & Monsignori-Fossi, B. C. 1996, ApJS, 106, 143
 Burgess, A., & Sheorey, B. V. 1974, J. Phys. B, 7, 2403
 Cheng, K. T., Kim, Y.-K., & Desclaux, J. P. 1979, Atom. Data Nucl. Data Tables, 24, 111

- Dere, K. P., Landi, E., Mason, H. E., Monsignori-Fossi, B. C., & Young, P. R. 1997, *A&AS*, 125, 149
- Dwivedi, B. N., & Raju, P. K. 1988, *Sol. Phys.*, 68, 111
- Edlen, B. 1983, *Phys. Scripta*, 28, 483
- Eissner, W., & Seaton, M. J. 1972, *J. Phys. B*, 5, 2187
- Eissner, W., Jones, M., & Nussbaumer, H. 1974, *Comput. Phys. Commun.*, 8, 270
- Foster, V. J., Keenan, F. P., & Reid, R. H. G. 1997, *Atom. Data Nucl. Data Tables*, 67, 99
- Harrison, R. A., et al. 1995, *Sol. Phys.*, 162, 233
- Kastner, S. O., & Bhatia, A. K. 1979, *A&A*, 71, 211
- Kaufman, V., & Martin, W. C. 1991, *J. Phys. Chem. Data*, 20, 130
- Keenan, F. P., Thomas, R. J., Neupert, W. M., & Conlon, E. S. 1994, *Sol. Phys.*, 149, 301
- Keenan, F. P., Thomas, R. J., Neupert, W. M., Conlon, E. S., & Burke, V. M. 1993, *Sol. Phys.*, 144, 69
- Martin, W. C., & Zalbulas, R. 1980, *J. Phys. Chem. Data*, 9, 42
- Merkelis, G., Vikas, M. J., Gaigalas, G., & Kisielius, R. 1994, *Phys. Scripta*, 51, 233
- Saraph, H. E. 1972, *Comput. Phys. Commun.*, 3, 256
- Thomas, R. J., & Neupert, W. M. 1994, *ApJS*, 91, 461
- Vernazza, J. E., & Mason, H. E. 1978, *ApJ*, 226, 720
- Vernazza, J. E., & Reeves, E. M. 1978, *ApJS*, 37, 485
- Young, P. R., Landi, E., & Thomas, R. J. 1998, *A&A*, 329, 291
- Zhang, H. L., & Sampson, D. H. 1994, *Atom. Data Nucl. Data Tables*, 56, 41